Nano Research 2018, 11(8): 4401–4411
https://doi.org/10.1007/s12274-018-2030-z
Research Article
ISSN 1998-0124
CN 11-5974/O4

Polarization effect in tip-enhanced infrared nanospectroscopy studies of the selective Y5 receptor antagonist Lu AA33810

Natalia Piergies[1,§] (✉), Ewa Pięta[1,§] (✉), Czesława Paluszkiewicz[1], Helena Domin[2], and Wojciech M. Kwiatek[1]

[1] *Institute of Nuclear Physics, Polish Academy of Sciences, PL-31342 Krakow, Poland*
[2] *Institute of Pharmacology, Polish Academy of Sciences, Department of Neurobiology, 31-343 Krakow, Smetna Street 12, Poland*
[§] *Natalia Piergies and Ewa Pięta contributed equally to this work.*

Received: 30 November 2017
Revised: 12 February 2018
Accepted: 18 February 2018

KEYWORDS
tip-enhanced infrared nanospectroscopy, polarization modulation, Y5 receptor antagonist, gold nanoparticles, adsorption

ABSTRACT

A novel approach of combining conventional infrared spectroscopy (IR) and atomic force microscopy (AFM) is presented to better understand the behavior of a drug adsorbed on a metal substrate at the nanoscale level. Tip-enhanced infrared nanospectroscopy (TEIRA) was used for the first time to investigate Lu AA33810, a selective brain-penetrating Y5 receptor antagonist, after immobilization on gold nanoparticles (GNPs). Here, a gold coated AFM tip and gold substrate were used to obtain the near-field electromagnetic field trapping effect. Because of the huge signal enhancement, it was possible to obtain the spectral information regarding the self-assembled monolayer of the investigated molecule. The effect of two orthogonal polarizations (*p*- and *s*-polarization modulations) of the excitation laser beam on the spectral patterns is also discussed. The results show that there is a strong relationship between the state of polarization of the incident radiation and the relative infrared band intensities. Another factor affecting the observed spectral differences is the topology of the metal substrate, which may result in the induction of a cross-polarization effect. The performed analysis indicates that the C–C bond from the cyclohexyl group is oriented almost parallel to the metal surface. Conversely, the *p*- and *s*-polarized spectral variations suggest that the O=S=O angle is high enough to enable the simultaneous interaction of both oxygen atoms with the GNPs.

1 Introduction

There is growing interest in the field of mid-infrared spectroscopy applications for thin objects at the nanoscale level [1, 2]. It is widely known that the infrared absorption of a molecule is greatly strengthened when it is immobilized onto, or is localized in close proximity, to a metal surface, such as Ag, Au, Cu, or In [3]. This phenomenon occurs in

Address correspondence to Natalia Piergies, natalia.piergies@ifj.edu.pl; Ewa Pięta, ewa.pieta@ifj.edu.pl

surface-enhanced infrared absorption (SEIRA) spectroscopy and was first observed in the attenuated-total reflection mode [4]. This enhancement effect is analogous to that observed in surface-enhanced Raman spectroscopy (SERS) [5–7]. The observed SERS bands are due to the changes in polarizability of the molecule, while the SEIRA signal is related to the variations in the molecule dipole moment [8]. Conversely, metal nanoparticles demonstrate unique properties, making them a very attractive material. Biocompatibility, functionality, lack of toxicity, and high surface-to-volume ratio are just a few advantages of these nanostructures [9]. Therefore, many applications have been found in biology and medicine, especially as drug sensors and delivery carriers [10], molecular imaging probes [11], or imaging agents [12]. It should be emphasized that nanoparticles are able to pass through the blood-brain barrier (BBB) by the endocytosis mechanism [13], also providing the opportunity to use them as biosensors for molecules with potential antidepressant activities.

There has recently been a major emphasis on the development of various spectroscopic techniques for obtaining nanometer resolution. In the previous paper we presented data that highlighted the role of radiation in the tracking of DNA damage at the nanoscale [14]. Conversely, Święch and co-workers demonstrated spectroscopic results for a biologically active molecule immobilized on colloidal nanoparticles [15]. In both experiments, tip-enhanced Raman spectroscopy (TERS), with the metal-coated tip acting as optical nanoantenna, induces the localized surface plasmon (LSP) effect to increase the sensitivity and spatial resolution of the spectral information. A similar situation is observed in the case of infrared nanospectroscopy with a gold coated tip. Lu and co-workers demonstrated that the use of a gold coated atomic force microscopy (AFM) tip, together with the gold coated surface, induces an optical field in the nanogap appearing between them [16, 17]. In the so-called tip-enhanced infrared nanospectroscopy (TEIRA) technique the local field intensity amplification increases the infrared absorption cross-section by over five orders of magnitude of that detected by the AFM tip.

The TEIRA phenomenon can be achieved by the use of IR spectroscopy combined with atomic force microscopy (AFM-IR) [16, 18, 19]. The AFM-IR technique incorporates all features and advantages that are supplied by AFM and IR separately [20]. Therefore, IR studies of the chemical composition and topography characterizations of the investigated samples can be performed. It is well-known that even Fourier-transform infrared spectroscopy (FT-IR) coupled with a microscope does not overcome the diffraction limit [21, 22]. Therefore, the highest possible spatial resolution is up to 1 μm [23, 24]. This limitation can be avoided using AFM-IR spectroscopy where the IR light induces a thermal expansion within the sample. The thermal expansion signal is detected by the AFM tip. Moreover, the tip is applied not only to probe, mapping the topography, but also to register the IR intensities [20, 25]. Because the spatial resolution is limited by the tip radius, the IR spectra of various materials with nanoscale resolution are currently available [26–28]. Another crucial AFM-IR feature is associated with the direct proportionality between the aforementioned thermal expansion and coefficient of absorption of the sample [25]. The sample thermal expansion is induced when the molecular vibrations return from the excited to the ground vibrational state upon energy transfer in the form of heat [29]. The occurrence of the excitation of the molecules modes is due to the absorption of IR photons emitted by the tunable laser. Because of this dependency the AFM-IR bands correlate to those obtained from the conventional transmission IR spectroscopy [25].

It is important to note that the AFM-IR spectra can be also employed for determining the molecular orientation by applying polarized IR excitation light [20, 25]. The polarization effect in the AFM-IR technique is similar to that occurring in the conventional IR method. Polarization modulation can be used to elucidate the chemical properties of studied molecules, which is not possible in the case of non-polarized light. There has long been an interest in studying the chemical bonding of various materials and discussing the molecular orientation onto metal surfaces [30]. It is important to note that the light phase after reflection from a metal surface depends on the angle of incidence and the state of polarization of the incident radiation [30, 31]. In the case of a high angle of incidence (grazing incidence), the absorption of *p*-polarized IR radiation by a thin layer on the metal surface is highly strengthened and even sub-monolayer quantities of chemisorbed molecules

can be observed in the *p*-polarized spectrum [32]. In contrast, for *s*-polarized radiation at the same high angle of incidence, virtually zero absorption is observed. This specific relation between *p*- and *s*-polarized excitation light induces special surface selection rules which can be used to determine the geometry of the monolayer of molecules immobilized onto the metal substrate [32]. Therefore, molecular dipole moments alongside the highly reflecting surface are not excited by *s*-polarized radiation at any incidence angle [33–35]. Additionally, the component of the dipole moments normal to this surface is excited by *p*-polarized excitation light for large incidence angles. Hence in the case of a *p*-polarized IR beam, the *x*- and *z*-components of the electric field are observed, while for the *s*-polarization beam, only the *y*-component is observed [31, 36].

It is commonly known that the topology of the metal substrate (e.g., metal nanoparticles and electrochemically roughened metal surface) noticeably affects the signal enhancement. As the wavelength of infrared radiation is much larger than the distance between metal nanoparticles, the surface optical properties of the metal are strongly dependent on the metal type, immobilized species, or surrounding medium [37]. Conversely, the polarizability of a metal particle is strongly associated with the nanoparticle shape and state of the polarization of the incident radiation [8]. For a proper analysis, the so-called surface selection rules must be taken into account. Accordingly, vibrations with dipole moment derivative components normal to the metal substrate are the most strengthened, while those oriented parallel will be absent or only slightly enhanced [8, 38]. This is due to the changes in the dipole moment that are enhanced alongside the surface normal. Therefore, the total dipole moments are doubled. Furthermore, the changes in the dipole moments across the surface normal are cancelled. This is because the dipole moment induced in the surface possesses the same magnitude but with an opposite direction [39]. As a consequence, it is possible to deduce the orientation of molecules adsorbed onto metal surfaces.

TEIRA investigations of N-[[trans-4-[(4,5-dihydro[1] benzothiepino[5,4-*d*]thiazol-2-yl)amino]cyclohexyl]methyl]-methanesulfonamide (Lu AA33810) are presented here: self-assembled monolayer immobilization on colloidal gold nanoparticles at the nanoscale level. Additionally, the influence of the use of two orthogonal polarizations (*p*- and *s*-) onto the individual band intensities resulting from the defined orientation, is characterized. Lu AA33810 is a highly selective and potent neuropeptide Y (NPY) Y5 receptor antagonist [40, 41] and its structure is showed in Fig. 1. It has been postulated that the NPY-ergic system is involved in the pathophysiology of depression [42, 43]. Since Lu AA33810 is a brain penetrant and low molecular weight compound, it is suitable for use in experimental models of mood disorders. Recent findings indicate that Lu AA33810, produces antidepressant-like effects in animal models of depression [40, 41, 44]; hence, a significant role of Y5 receptors in depression-related disorders has been postulated. Nevertheless, the utility of Y5R ligands as therapeutics is still limited and there is a need for the discovery of more brain penetrant Y5R antagonists to better define the role of these receptors in the central nervous system. Therefore, knowledge of the molecular structure/bioactivity relationship of Lu AA33810 is important in order to design new compounds with antagonist properties similar to Y5R.

In the recent study, the molecular structure of Lu AA33810 was determined experimentally (Raman spectroscopy (RS) and FT-IR and theoretically (density functional theory (DFT)) [45]. Furthermore, SERS and SEIRA techniques have been used to discuss the Lu AA33810 interfacial behavior onto GNPs surfaces. It was implied that thiazole (Thz) and phenyl (Phe) rings play a dominant role in the adsorption phenomenon, emphasizing the interaction between the free electron pair from Thz and the gold nanoparticles surface. The charge transfer (CT) mechanism had a significant

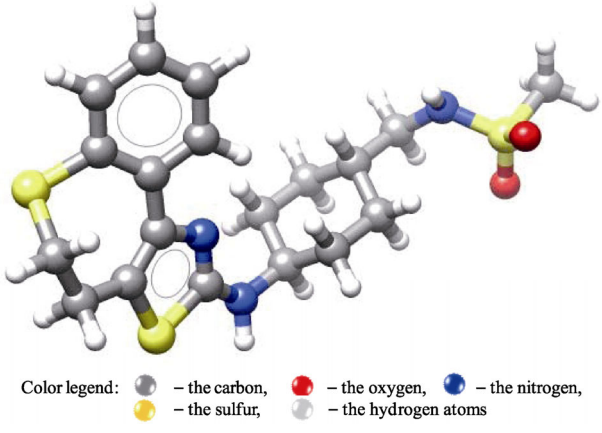

Figure 1 Optimized structure of Lu AA33810.

impact on the Raman signal enhancement. Additionally, the observed changes proved the existence of an interaction between the free electron pairs located on oxygen atoms from SO_2 moiety and GNPs. It was also noted that the NH fragment from 2-aminothiazole and/or methanesulfonamide was situated in some proximity to the metal substrate. Moreover, our previous investigations provided information regarding the mode of adsorption of NPY and its native NPY3–36, NPY13–36, and NPY22–36, as well as mutated acetyl-(Leu28,31)-NPY24–36 C-terminal fragments [46].

To the best of our knowledge, this is the first report to present a novel approach for studying the molecule orientation on a metal nanostructure, by employing the thermal expansion effect. Previous research has demonstrated the application of metal plasmonic resonators to achieve local absorption enhancement in the mid-IR spectral region with nanoscale resolution [47, 48]. Nevertheless, in this study, we used metal nanoparticles to obtain the local field enhancement and describe the behavior of the Lu AA33810 monolayer after conjugation with the substrate. This was demonstrated by using the infrared nanospectroscopy technique with the polarized light illuminating the sample from above.

2 Experimental

2.1 Sample preparation

Lu AA33810 was purchased from Tocris Bioscience (UK) (purity ~ 98.3%) and prepared according to previously published data [45]. A freshly prepared aqueous solution was obtained by dissolving 2.13 mg of the investigated antagonist in the deionized water using the sonification process. The concentration of the solution was ~ 0.1 mM.

2.2 Gold nanoparticles synthesis

The gold nanoparticle suspension (TC-GNPs) was synthesized according to the previously published procedure [49]. 108 mL of aqueous solution containing 0.93 mM of hydrogen tetrachloroaurate and 2.89 mM of trisodium citrate was heated at 88 ˚C for 15 min. The mass concentration of the nanoparticles in the prepared colloidal solution was defined using DMA 5000M equipment from the Anton Paar Company and was 122 mg·L^{-1}.

2.3 Tip-enhanced infrared nanospectroscopy studies

Prior to the measurements, 33 μL of the TC-GNPs was mixed with 33 μL of the Lu AA33810 solution. For a better colloid aggregation, a 0.1 M concentration NaCl solution was added. The prepared liquid mixture was placed onto CaF_2 windows and used for further investigations after it was dried. The tip-enhanced spectra at nanoscale resolution were collected from five different areas by means of the NanoIR2 Anasys Instrument (a schematic representation is shown in Fig. 2).

The optical parametric oscillator (OPO) laser with a spectral range of 3,350–1,000 cm^{-1} was applied as an infrared source. A laser with a nominal incident power of 8 mW, during the measurements, was set to use 17% of the incident power. The nanoscale AFM-IR spectra were collected with 4 cm^{-1} spectral resolution and each data point was obtained by averaging 256 pulses of excitation. The spectral bands from the measured series of spectra were almost identical and only slight changes in some of the relative intensities (up to 5%) were observed. For all spectra, a smoothing with the Savitzky-Golay algorithm (second order, three points) and a multipoint baseline correction (five points) were performed. It should be emphasized that the relative intensities of the bands were not affected by these procedures.

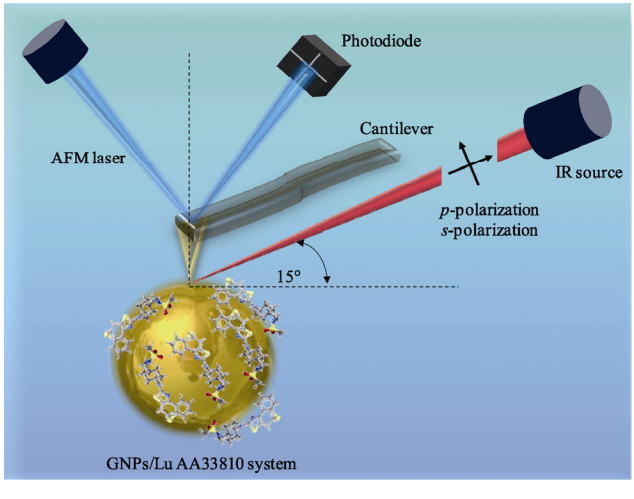

Figure 2 Scheme of TEIRA experiment.

The topography of the investigated Lu AA33810/GNPs system was collected in the tapping mode by use of cantilevers with a spring constant of 1 $N \cdot m^{-1}$ and resonance frequency of 75 kHz (the resolution in both the x and y directions was 128). The topographic images were taken before and after collection of each of the series of spectra in order to control thermal expansion effects on the sample. During the AFM-IR experiments, no thermal modifications within the sample were observed.

2.4 Fitting procedure

Fitting of the 1,400–1,225 cm^{-1} and 1,250–975 cm^{-1} spectral regions for the TEIRA spectra of the investigated molecule collected using p- and s-polarization, respectively, was conducted using OMNIC software. A Gaussian band shape was assumed and fixed for all bands.

3 Results and discussion

Figure 3 shows the TEIRA spectra of the Lu AA33810 after immobilization onto TC-GNPs collected for p- (Fig. 3(a)) and s-polarization radiation Fig. 3(b), respectively. From each sample area, the fifty spectra were collected in different positions (see Fig. 4(a) for the AFM image).

The spectra were collected at each position using p- and s-polarization modulations. The most reproducible spectra for further analysis were selected. The depth histogram (Fig. 4(b)) together with the horizontal and vertical height profiles (Figs. 4(c) and 4(d), respectively) indicate that the high differentiation observed for the selected area of the sample is about 290 nm. The observed spectral patterns show crucial variations in the band relative intensities as a consequence of the light polarization modulation. As discussed in the Introduction, the polarized incident field induces excitation only for vibrations in which the dipole moment is aligned with the applied polarization [50]. Therefore, the NanoIR2 system, with the IR-tunable laser located at 75° to the surface normal (see Fig. 2) and polarization parallel to the tip axis (p-polarized light), should provide the enhancement of vibrations with dipoles oriented perpendicular to the metal nanostructure. Conversely, for the orthogonal polarization modulation (s), the bands due to the bonds situated tilted or almost parallel to the metal surface should be visible. These effects could not be observed by using conventional infrared spectroscopy in the transmission mode [8].

These results are constituent with the data published

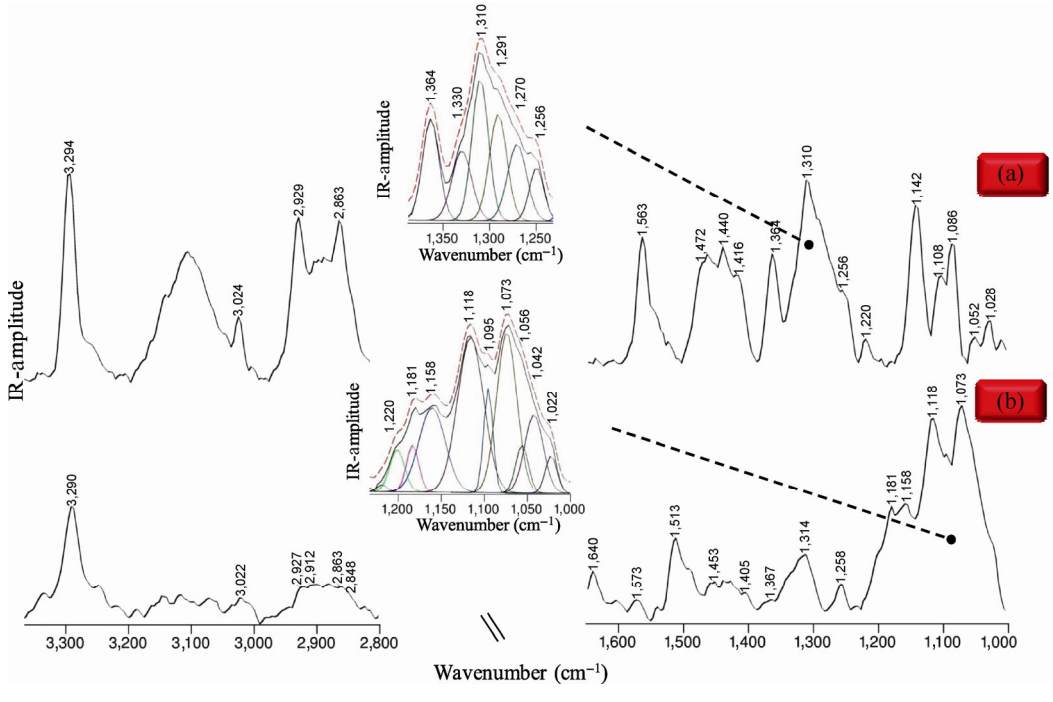

Figure 3 TEIRA spectra of Lu AA33810 immobilized onto TC-GNPs recorded using p- and s-polarization ((a) and (b), respectively) with the appropriate curve fitting; the black solid and red dotted lines are the original and composite result spectra, respectively. IR source: optical parametric oscillator laser; spectral resolution = 4 cm^{-1}.

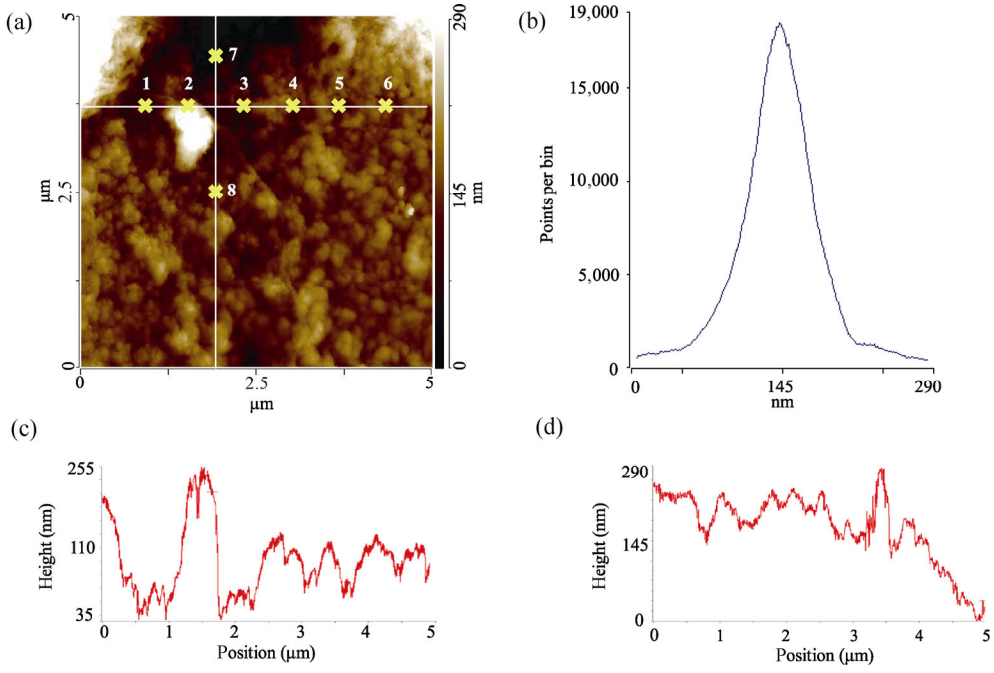

Figure 4 AFM image: 5 μm × 5 μm of the GNPs/Lu AA33810 system. (a) The depth histogram and (b) horizontal and vertical height profiles ((c) and (d), respectively). The AFM image was processed by flattening. Topography collection: tapping mode.

by Osawa and co-workers; a significant decrease (1/5) of the SEIRA intensities with changing polarization from *p* to *s* was observed [8, 38]. Moreover, Ataka and co-authors suggested a reduction of the SEIRA signal to 1/20 upon polarization variation [37]. In our experiment, the estimated reduction factor for the relative intensities of the corresponding TEIRA bands is 1/14. In the high wavenumber range, this is manifested by the dramatic decrease in the $CH_3/CH_2/CH$ vibrational modes intensities for the spectra collected with *s*-polarized IR light. This phenomenon coupled with the observed strengthening of the aforementioned bands suggest a rather perpendicular orientation of the C–H bonds on the metal surface. However, there are significant differences between the *p*-polarized TEIRA signal and conventional SEIRA bands recorded in the transmission mode [45]. In particular, the bands at 2,954 and 2,851 cm^{-1} in the SEIRA spectrum [45], attributed to the asymmetric CH_3 and symmetric CH_2 stretching modes, are not observed in the *p*-polarized nanoscale signal. These findings confirm that the intensities of the C–H bands reveal a strong polarization dependence [36, 51]. A different spectral pattern is observed for the amino group. Here, the TEIRA *p*- and *s*-polarized spectral features at 3,294 and 3,290 cm^{-1} due to the NH stretching oscillations exhibit a noticeable red shift ($\Delta\bar{\nu}$ = 3 cm^{-1} and $\Delta\bar{\nu}$ = 7 cm^{-1}, respectively) in comparison to the corresponding SEIRA spectrum [45]. The wavenumber assignments are given in Table 1.

Furthermore, there is a good correlation between the *p*-polarized TEIRA spectrum and previously published SEIRA spectrum [45]. This is consistent with the above discussed relation between the polarization state and IR signals intensities. Accordingly, the strongest band intensities for the molecule adsorbed onto the metal surface are observed for the IR beam polarized parallel to the incidence plane [31, 35, 36]. This TEIRA spectrum is dominated by spectral features attributed to the Thz ring vibrations at 1,584 cm^{-1} (ν(CC)), 1,563 cm^{-1} (ν(CC)), 1,541 cm^{-1} ($\nu(CC)_{Phe/Thp/Thz}$, ρ_b(NH), ν(CN)), 1,465 cm^{-1} ($\nu(CC)_{Phe/Thp}$, $\rho_b(CH)_{Phe}$, ρ_b(NH)), 1,416 cm^{-1} (ρ_b(NH)), 1,364 cm^{-1} (ν_s(C=C), ν_s(C=N), ρ_b(NH)), 1,330 cm^{-1} (ν(CN)), 1,310 cm^{-1} (ν(C=N)), 1,291 cm^{-1} ($\nu(CN)_{Thz\text{-}NH}$), 1,181 cm^{-1} ($\nu(CN)_{Thz\text{-}NH}$), 1,142 cm^{-1} (δ(Thz)), and 1,108 cm^{-1} ($\nu(CN)_{Thz/Thz\text{-}NH}$) (Table 1).

These bands exhibit a slight decrease in the relative intensities upon *p*-polarized IR excitation (Figs. 2(c) and 2(d)). This confirms the previous analysis indicating that the Thz aromatic moiety accepts a tilted orientation onto the GNPs, leading to interaction with the Thz free electron pair [45]. However, for the *p*-polarized TEIRA signals at 1,310 and 1,142 cm^{-1}, attributed to

Table 1 Wavenumber and band assignments for the SEIRA and TEIRA spectra of Lu AA33810 adsorbed on TC-GNPs surface according to Ref. [45][a]

Assignment	Wavenumber (cm^{-1})		
	SEIRA	TEIRA	
		p-polarization	*s*-polarization
ν(NH)	3,297	3,294	3,290
$\nu(CH)_{ring}$	3,048	—	—
ν(CH)	3,026	3,024	3,022
$\nu_{as}(CH_3)$	2,954	—	2,954
$\nu_{as}(CH_2)$	2,924	2,929	2,927
$\nu_s(CH_3)$	2,865	2,863	2,863
$\nu_s(CH_2)$	2,851	—	2,848
δ(NH)	1,632	1,637	1,640
$\nu(CC)_{Phe/Thp/Thz}$	1,584	1,584	1,596
$\nu(CC)_{Phe/Thp/Thz}$	1,565	1,563	1,573
$\nu(CC)_{Phe/Thp/Thz}$, ρ_b(NH), ν(CN)	1,539	1,541	1,542
ν(CN), δ(NH)	1,509	1,509	1,513
$\rho_s(CH_2)$	1,474	1,472	—
$\nu(CC)_{Phe/Thp}$, $\rho_b(CH)_{Phe}$, ρ_b(NH)	1,465	1,465	1,453
$\rho_b(CH_2)$	1,438	1,440	1,440
ρ_b(NH)	1,421	1,416	1,427
$\rho_b(CH_3)_{as}$, $\rho_b(NH)_{MSA}$	—	—	1,405
ν_s(C=C), ν_s(C=N), ρ_b(NH)	1,365	1,364	1,367
ν(CN), $\rho_w(CH_2)_{chx}$, $\nu(CC)_{chx}$, $\rho_b(NH)_{MSA}$	1,330	1,330	1,332
$\nu_{as}(SO_2)$	1,320	—	1,322
ν_s(C=N), $\nu(CC)_{Phe/Thp}$	1,306	1,310	—
$\nu(CC)_{Phe/Thp}$, $\rho_b(CH)_{Phe}$, $\rho_w(CH_2)_{Thp}$, $\nu(CN)_{Thz\text{-}NH}$, $\rho_r(CH_2)_{chx}$	1,301	1,291	—
$\delta(CH_2)$, $\rho_b(CH)_{Phe}$	1,253	1,256	1,258
$\rho_b(CH)_{Phe}$, δ(Phe), $\rho_t(CH_2)_{Thp}$, $\rho_t(CH_2)_{chx}$, δ(Thz), ν(NC), δ(Thp)	1,220	1,220	1,220
$\rho_t(CH_2)_{Thp}$, $\delta(CH_2)_{Phe/Thp}$, $\nu(CN)_{Thz\text{-}NH}$	1,179	1,181	1,181
$\nu_s(SO_2)$	1,153	—	1,158
δ(Thz)	1,144	1,142	—
$\nu(CN)_{Thz/Thz\text{-}NH}$, $\rho_r(CH)_{Phe}$, $\rho_w(CH_2)_{Thp}$	1,109	1,108	1,118
$\nu_s(SO_2)$, $\rho_w(CH_3)$	1,093	1,086	1,095
$\nu(CC)_{chx}$	1,068	—	1,073
$\nu(CC)_{chx}$, $\nu(CC)_{Phe}$, $\rho_r(CH_2)_{chx}$, $\rho_r(CH)_{Phe}$, $\nu_s(SO_2)$, $\rho_w(CH_2)_{Thp}$	1,054	1,052	1,056
Phe_{breath}	1,035	1,032	1,042
$\nu(CC)_{chx}$, $\nu(CN)_{MSA}$	1,023	1,028	1,022

[a]Abbreviations: ν, stretching; δ, deformation; ρ_b, bending; ρ_s, scissoring; ρ_w, wagging; ρ_t, twisting; ρ_r, rocking; as, asymmetric; breath, breathing; Phe, phenyl; chx, cyclohexyl; Thp, thiepine; Thz, thiazole; MSA, methanesulfonamide.

the C=N stretching and Thz deformation vibrations, respectively, a significant enhancement is noticed. This suggests that the tilted orientated Thz ring forces the perpendicular arrangement of the C=N double bond. Additionally, the C–N single bond is located almost parallel to the metal surface, confirmed by the strong intensity of the 1,118 cm^{-1} band in the *s*-polarized register signal. Further evidence for this is the 1,513 and 1,181 cm^{-1} spectral features (Table 1) present in the *s*-polarized spectrum that are invisible in the *p*-polarized

spectral patterns.

It should also be noted that the benzothiepine (Phe-Thp) oscillations appearing at 1,256 cm^{-1} ($\delta(CH_2)$, $\rho_b(CH)_{Phe}$), 1,220 cm^{-1} ($\delta(CH_2)$, $\rho_b(CH)_{Phe}$), and 1,028 cm^{-1} (Phe_{breath}) in the *p*-polarized TEIRA spectrum are noticeably weakened in comparison with the conventional SEIRA spectrum. Furthermore, significant enhancement of the above-listed bands in the *s*-polarized spectrum is observed. Consequently, the Phe-Thp group is tilted towards the metal surface, while the tilt angle between this moiety and the surface is smaller than that observed in the case of Thz.

As discussed above, for *s*-polarization modulation, the highest IR absorption is expected for molecular vibrations with dipole derivatives parallel or tilted to the surface plane. Regarding the spectral features observed in the *s*-polarized TEIRA spectrum, it could be assumed that the C–C bond from cyclohexyl is localized almost parallel with regard to the metal surface. This is manifested by the presence of the greatly strengthened band at 1,073 cm^{-1} ($\nu(CC)_{chx}$, $\rho_b(CH)$). It should be noted that the aforementioned modes are not observed in the corresponding *p*-polarized spectrum.

Moreover, the enhancement of the *s*-polarized bands due to the SO_2 stretching vibrations appearing at 1,322 cm^{-1} ($\nu_{as}(SO_2)$), 1,158 cm^{-1} ($\nu_s(SO_2)$), 1,095 cm^{-1} ($\nu_s(SO_2)$), and 1,056 cm^{-1} ($\nu_s(SO_2)$) cannot be omitted. It may suggest that the S–O bond adopts a tilted orientation onto the studied metal substrate. This statement is further supported by the significant relative intensity decrease of these bands in the *p*-polarized spectrum. As was discussed in the previously published results [45], the methanesulfonamide moiety from the investigated antagonist interacts with GNPs via the free electron pairs situated on the oxygen atoms from the SO_2 moiety. The spectral patterns observed in the *p*- and *s*-polarized spectra indicate that both oxygen atoms from the O=S=O fragment interact with the metal surface.

Figures 5 and 6 show the *p*- and *s*-polarized spectra collected from eight different positions marked in the 5 μm × 5 μm AFM image (Fig. 4(a)).

Some slight differences were observed for the relative band intensities. The enhancement of the ~ 1,028 cm^{-1} *p*-polarized band and simultaneous decrease of the ~ 1,072 cm^{-1} *s*-polarized signal indicate that the angle between the C–C bond from cyclohexyl and metal plane slightly increased in some positions.

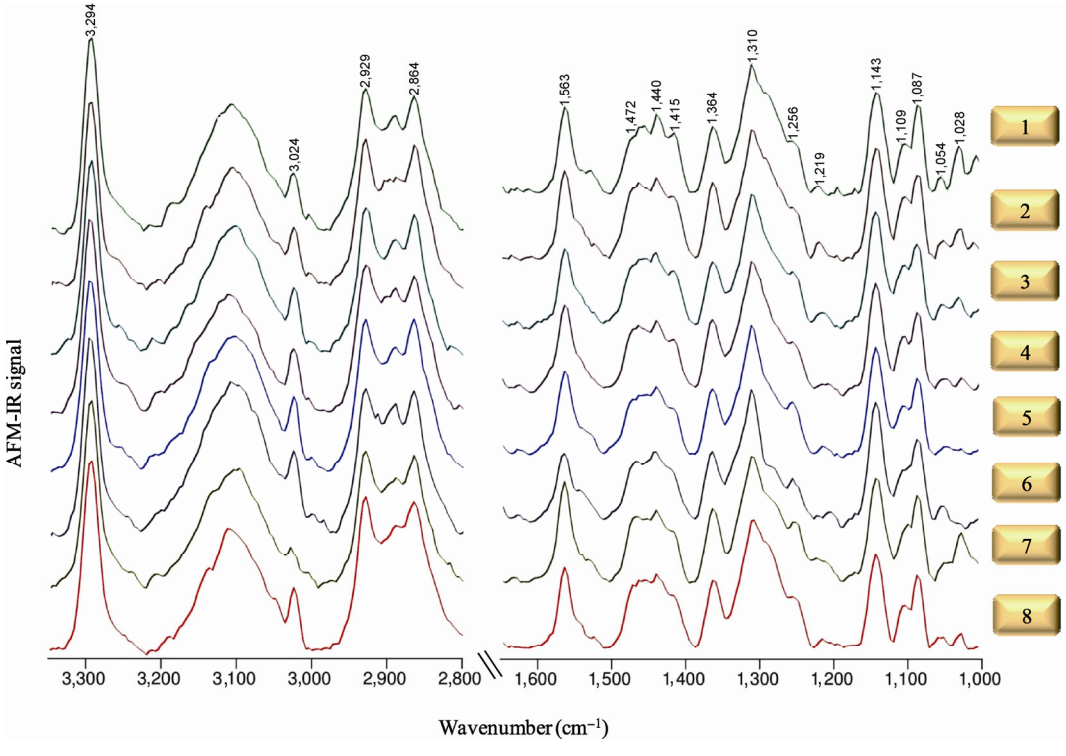

Figure 5 TEIRA spectra of Lu AA33810 immobilized onto the TC-GNPs surface recorded using *p*-polarization. The spectra were normalized using the min–max normalization procedure. IR source: optical parametric oscillator laser; spectral resolution = 4 cm^{-1}.

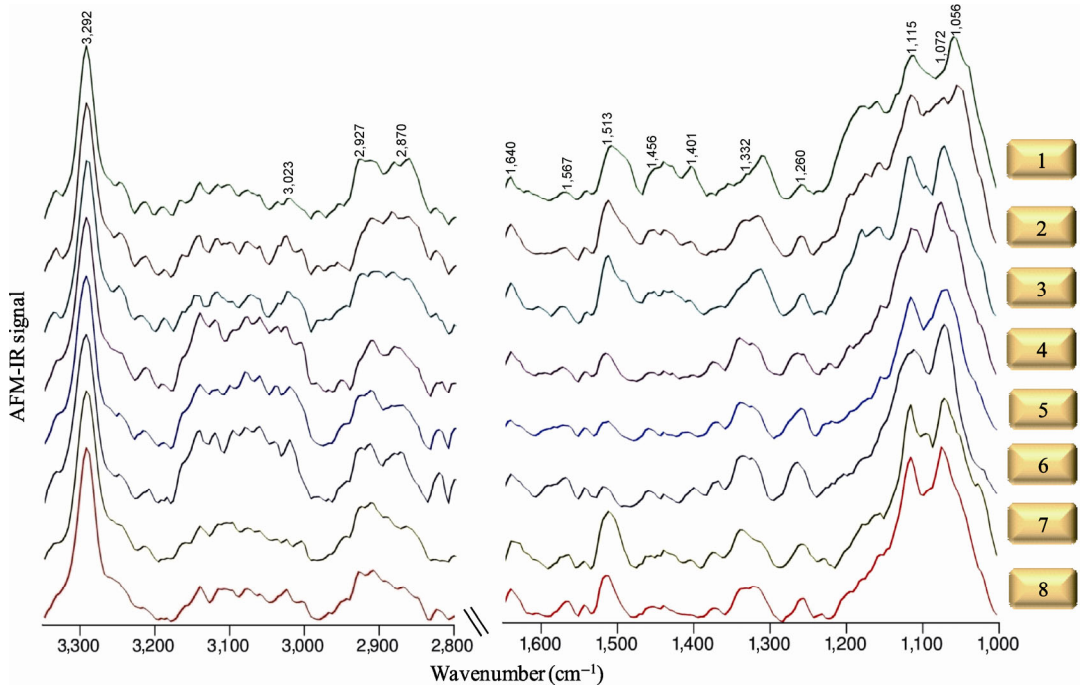

Figure 6 TEIRA spectra of Lu AA33810 immobilized onto the TC-GNPs surface recorded using *s*-polarization. The spectra were normalized using the min–max normalization procedure. IR source: optical parametric oscillator laser; spectral resolution = 4 cm^{-1}.

The situation is somewhat different for the C–N bond from the Thz and SO_2 moiety, where a more parallel orientation for these two fragments was expected. This finding can be supported by noticeable variations of the 1,513, 1,332, 1,158, 1,115, and 1,056 cm^{-1} bands intensities in *s*-polarization (see Table 1 for the assignments). The observed differentiation is a likely consequence of the irregular substrate, forming large aggregates containing bifurcations and protrusions. This anisotropy may induce a cross-polarization effect, affecting the variations in the spectral signals [52].

4 Conclusions

We presented the first TEIRA results obtained for the Lu AA33810 monolayer adsorbed on gold nanoparticles at the nanoscale level. From these results, we conclude that a combination of classical IR spectroscopy with AFM enabled better monitoring of the adsorption process of the investigated molecule. The application of the gold coated AFM tip allowed the detection of local thermal expansion within the sample and the additional near-field electromagnetic field trapping effect. This phenomenon results from the optical field induced in the nanogap between the gold tip and gold nanostructure. The effect of two orthogonal polarizations (*p*- and *s*-polarized exciting laser beam) on the spectral feature changes was also considered. There was a strong dependence of the state of polarization of the incident radiation on the spectral pattern changes associated with the defined molecular orientation. The observed spectral variations at some points of the investigated areas may be due to the irregular surface creating large aggregates with numerous bifurcations and protrusions. Therefore, such differences may be related to the cross-polarization effect.

From the performed analysis, it is possible to conclude that the C–C bond from the cyclohexyl moiety adopts an almost parallel position on the GNPs surface. Furthermore, it can be stated that the O=S=O angle is large enough for the simultaneous interaction of both oxygen atoms with the gold substrate. The observation of the tilted oriented Phe-Thp moiety demonstrated that the tilt angle between this group and the GNPs is smaller than that observed for the Thz ring, forcing the perpendicular arrangement of the C=N double bond. It should be emphasized that the application of the IR exciting light in two orthogonal polarization modulations provides a more precise characterization of the adsorption geometry of the investigated molecule.

Acknowledgements

The research was performed by the use of the equipment purchased in the frame of the project co-funded by the Małopolska Regional Operational Program Measure 5.1 Krakow Metropolitan Area as an important hub of the European Research Area for 2007–2013 (No. MRPO.05.01.00–12–013/15). This work was also supported by the National Science Centre Poland (No. 2016/21/D/ST4/02178 to N. P. and 2017/01/X/ST4/00428 to E. P.). The authors gratefully acknowledge M. Oćwieja, Ph. D, J. Haber Institute of Catalysis and Surface Chemistry, Polish Academy of Sciences, for GNPs synthesis.

References

[1] Goswami, A.; Dhandaria, P.; Pal, S.; McGee, R.; Khan, F.; Antić, Z.; Gaikwad, R.; Prashanthi, K.; Thundat, T. Effect of interface on mid-infrared photothermal response of MoS_2 thin film grown by pulsed laser deposition. *Nano Res.* **2017**, *10*, 3571–3584.

[2] Vitry, P.; Rebois, R.; Bourillot, E.; Deniset-Besseau, A.; Virolle, M. J.; Lesniewska, E.; Dazzi A. Combining infrared and mode synthesizing atomic force microscopy: Application to the study of lipid vesicles inside *Streptomyces* bacteria. *Nano Res.* **2016**, *9*, 1674–1681.

[3] Aroca, R. F.; Ross, D. J.; Domingo, C. Surface-enhanced infrared spectroscopy. *Appl. Spectrosc.* **2004**, *58*, 324A–338A.

[4] Hartstein, A.; Kirtley, J. R.; Tsang, J. C. Enhancement of the infrared absorption from molecular monolayers with thin metal overlayers. *Phys. Rev. Lett.* **1980**, *45*, 201–204.

[5] Qian, H. M.; Xu, M.; Li, X. W.; Ji, M. W.; Cheng, L.; Shoaib, A.; Liu, J. J.; Jiang L.; Zhu, H. S.; Zhang, J. T. Surface micro/nanostructure evolution of Au–Ag alloy nanoplates: Synthesis, simulation, plasmonic photothermal and surface-enhanced Raman scattering applications. *Nano Res*. **2016**, *9*, 876–885.

[6] Khlebtsov, B.; Khanadeev, V.; Khlebtson, N. Surface-enhanced Raman scattering inside Au@Ag core/shell nanorods. *Nano Res*. **2016**, *9*, 2303–2318.

[7] Wang, Y. D.; Lu, N.; Wang, W. T.; Liu, L. X.; Feng, L. F.; Zeng, Z. F.; Li, H. B.; Xu, W. Q.; Wu, Z. J.; Hu, W. et al. Highly effective and reproducible surface-enhanced Raman scattering substrates based on Ag pyramidal arrays. *Nano Res.* **2013**, *6*, 159–166.

[8] Osawa, M. Surface-enhanced infrared absorption. In *Near-Field Optics and Surface Plasmon Polaritons*; Kawata, S., Ed.; Springer-Verlag: Berlin, Heidelberg, 2001; pp 163–187.

[9] Joshi, P.; Chakraborti, S.; Ramirez-Vick, J. E.; Ansari, Z. A.; Shanker, V.; Chakrabarti, P.; Singh, S. P. The anticancer activity of chloroquine-gold nanoparticles against MCF-7 breast cancer cells. *Colloid. Surface B* **2012**, *95*, 195–200.

[10] Brigger, I.; Dubernet, C.; Couvreur, P. Nanoparticles in cancer therapy and diagnosis. *Adv. Drug Deliver Rev.* **2012**, *64*, 24–36.

[11] El-Ansary, A.; Faddah L. M. Nanoparticles as biochemical sensors. Nanotechnol. *Sci. Appl*. **2010**, *3*, 65–76.

[12] Wang, E. C.; Wang A. Z. Nanoparticles and their applications in cell and molecular biology. *Integr. Biol.* **2014,** *6*, 9–26.

[13] Kreuter, J. Drug delivery to the central nervous system by polymeric nanoparticles: What do we know? *Adv. Drug Deliver Rev.* **2014**, *71*, 2–14.

[14] Lipiec, E.; Sekine, R.; Bielecki, J.; Kwiatek, W. M.; Wood, B. R. Molecular characterization of DNA double strand breaks with tip-enhanced Raman scattering. *Angew. Chem.* **2014**, *126*, 173–176.

[15] Święch, D.; Ozaki, Y.; Kim, Y.; Proniewicz, E. Surface- and tip-enhanced Raman scattering of bradykinin onto the colloidal suspended Ag surface. *Phys. Chem. Chem. Phys.* **2015**, *17*, 17140–17149.

[16] Lu, F.; Jin, M. Z.; Belkin, M. A. Tip-enhanced infrared nanospectroscopy via molecular expansion force detection. *Nat. Photonics* **2014**, *8*, 307–312.

[17] Ruggeri, F. S.; Vieweg, S.; Cendrowska, U.; Longo, G.; Chiki, A.; Lashuel, H. A.; Dietler G. Nanoscale studies link amyloid maturity with polyglutamine diseases onset. *Sci. Rep.* **2016**, *6*, 31155.

[18] Dazzi, A.; Prazeres, R.; Glotin, F.; Ortega, J. M. Local infrared microspectroscopy with subwavelength spatial resolution with an atomic force microscope tip used as a photothermal sensor. *Opt. Lett.* **2005**, *30*, 2388−2390.

[19] Dazzi, A.; Prazeres, R.; Glotin, F.; Ortega, J. M. Subwavelength infrared spectromicroscopy using an AFM as a local absorption sensor. *Infrared Phys. Technol.* **2006**, *49*, 113−121.

[20] Dazzi, A.; Prater, C. B. AFM-IR: Technology and applications in nanoscale infrared spectroscopy and chemical imaging. *Chem. Rev*. **2017**, *117*, 5146–5173.

[21] Petibois, C.; Piccinini, M.; Guidi, M. C.; Marcelli, A. Facing the challenge of biosample imaging by FTIR with a synchrotron radiation source. *J. Synchrotron Rad.* **2010**, *17*, 1–11.

[22] Nasse, M. J.; Walsh, M. J.; Mattson, E. C.; Reininger, R.; Kajdacsy-Balla, A.; Macias, V.; Bhargava, R.; Hirschmugl, C. J. High-resolution Fourier-transform infrared chemical imaging with multiple synchrotron beams. *Nat. Methods* **2011**, *8*, 413–416.

[23] Reddy, R. K.; Walsh, M. J.; Schulmerich, M. V.; Carney, P. S.; Bhargava, R. High-definition infrared spectroscopic imaging. *Appl. Spectrosc.* **2013**, *67*, 93−105.

[24] Findlay, C. R.; Wiens, R.; Rak, M.; Sedlmair, J.; Hirschmugl, C. J.; Morrison, J.; Mundy, C. J.; Kansiz, M.; Gough, K. M. Rapid biodiagnostic *ex vivo* imaging at 1 μm pixel resolution with thermal source FTIR FPA. *Analyst* **2015**, *140*, 2493−2503.

[25] Dazzi, A.; Prater, C. B.; Hu, Q. C.; Chase, D. B.; Rabolt, J. F.; Marcott, C. AFM-IR: Combining atomic force microscopy and infrared spectroscopy for nanoscale chemical characterization. *Appl. Spectrosc.* **2012**, *66*, 1365–1384.

[26] Centrone, A.; Lahiri, B.; Holland, G. E. Chemical imaging beyond the diffraction limit using photothermal induced resonance microscopy. *Microsc. Anal.* **2013**, *27*, 6–9.

[27] Ruggeri, F. S.; Habchi, J.; Cerreta, A.; Dietler, G. AFM-based single molecule techniques: Unraveling the amyloid Pathogenic Species. *Curr. Pharm. Design* **2016**, *22*, 3950–3970.

[28] Paluszkiewicz, C.; Piergies, N.; Chaniecki, P.; Rękas, M.; Miszczyk, J.; Kwiatek, W. M. Differentiation of protein secondary structure in clear and opaque human lenses: AFM–IR studies. *J. Pharmaceut. Biomed.* **2017**, *139*, 125–132.

[29] Jackson, M.; Mantsch, H. H. The use and misuse of FTIR spectroscopy in the determination of protein structure. *Crit. Rev. Biochem. Mol.* **1995**, *30*, 95–120.

[30] Greenler, R. G. Infrared study of adsorbed molecules on metal surfaces by reflection techniques. *J. Chem. Phys.* **1966**, *44*, 310–315.

[31] Ras, H. A. R.; Schoonheydt, R. A.; Johnston, C. T. Relation between s-polarized and p-polarized internal reflection spectra: Application for the spectral resolution of perpendicular vibrational modes. *J. Phys. Chem. A* **2007**, *111*, 8787–8791.

[32] Frey, B. L.; Corn, R. M.; Weibel, S. C. Polarization-modulation approaches to reflection-absorption spectroscopy. In *Handbook of Vibrational Spectroscopy*; Griffiths, P. R., Ed.; John Wiley & Sons: New York, 2001; pp 1042–1056.

[33] Paluszkiewicz, C.; Handke, M.; Aleksandrowicz, R. Application of FT-IR spectroscopy to phosphate coatings on electrotechnical iron sheets. *J. Mol. Structure* **1984**, *114*, 433–436.

[34] Handke, M.; Paluszkiewicz, C. FTIR spectra of thin inorganic coatings on metals. *Infrared Phys.* **1984**, *24*, 121–128.

[35] Handke, M.; Milosevic, M.; Harrick, N. J. External reflection Fourier transform infrared spectroscopy: Theory and experimental problems. *Vibrat. Spectrosc.* **1991**, *1*, 251–262.

[36] Guo, P.-F.; Huang, W.-Y.; Liu, H.-B.; Xiao, S.-J. AFM and multiple transmission-reflection infrared spectroscopy (MTR-IR) studies on formation of air-stable supported lipid bilayers. *Int. J. Mol. Sci.* **2009**, *10*, 1407–1418.

[37] Ataka, K.; Stripp, S. T.; Heberle, J. Surface-enhanced infrared absorption spectroscopy (SEIRAS) to probe monolayers of membrane proteins. *Biochim. Biophys. Acta* **2013**, *1828*, 2283–2293.

[38] Osawa, M.; Ataka, K.; Yoshii, K.; Yotsuyanagi, T. Surface-enhanced infrared ATR spectroscopy for *in situ* studies of electrode/electrolyte interfaces. *J. Electron Spectrosc. Related Phenomena* **1993**, *64–65*, 371–379.

[39] Aroca, R. SERS/SERRS, the analytical tool. In *Surface-Enhanced Vibrational Spectroscopy*; Aroca, R., Ed.; John Wiley & Sons Ltd: Chichester, UK, 2006; pp 164–176.

[40] Walker, M. W.; Wolinsky, T. D.; Jubian, V.; Chandrasena, G.; Zhong, H. L.; Huang, X. Y.; Miller, S.; Hegde, L. G.; Marsteller, D. A.; Marzabadi, M. R. et al. The novel neuropeptide Y Y_5 receptor antagonist Lu AA33810 [N-[[trans-4-[(4,5-dihydro[1]benzothiepino[5,4-*d*]thiazol-2-yl)amino]cyclohexyl]methyl]-methanesulfonamide] exerts anxiolytic- and antidepressant-like effects in rat models of stress sensitivity. *J. Pharmacol. Exp. Ther.* **2009**, *328*, 900–911.

[41] Packiarajan, M.; Marzabadi, M. R.; Desai, M.; Lu, Y. L.; Noble, S. A.; Wong, W. C.; Jubian, V.; Chandrasena, G.; Wolinsky, T. D.; Zhong, H. L. et al. Discovery of Lu AA33810: A highly selective and potent NPY5 antagonist with *in vivo* efficacy in a model of mood disorder. *Bioorg. Med. Chem. Lett.* **2011**, *21*, 5436–5441.

[42] Heilig, M. The NPY system in stress, anxiety and depression. *Neuropeptides* **2004**, *38*, 213–224.

[43] Morales-Medina, J. C.; Dumont, Y.; Quirion, R. A possible role of neuropeptide Y in depression and stress. *Brain Res.* **2010**, *1314*, 194–205.

[44] Domin, H.; Szewczyk, B.; Pochwat, B.; Woźniak, M.; Śmiałowska, M. Antidepressant-like activity of the neuropeptide Y Y_5 receptor antagonist Lu AA33810: Behavioral, molecular, and immunohistochemical evidence. *Psychopharmacology.* **2017**, *234*, 631–645.

[45] Pięta, E.; Piergies, N.; Oćwieja, M.; Domin, H.; Paluszkiewicz, C.; Bielańska, E.; Kwiatek, W. M. Monitoring the interfacial behavior of selective Y5 receptor antagonist on colloidal gold nanoparticle surfaces: Surface-enhanced vibrational spectroscopy studies. *J. Phys. Chem. C* **2017**, *121*, 17276–17288.

[46] Domin, H.; Pięta, E.; Piergies, N.; Święch, D.; Kim, Y. Proniewicz, L. M.; Proniewicz, E. Neuropeptide Y and its C-terminal fragments acting on Y2 receptor: Raman and SERS spectroscopy studies. *J. Colloid Interf. Sci.* **2015**, *437*, 111–118.

[47] Lahiri, B.; Holland, G.; Aksyuk, V.; Centrone, A. Nanoscale imaging of plasmonic hot spots and dark modes with the photothermal-induced resonance technique. *Nano Lett.* **2013**, *13*, 3218−3224.

[48] Chae, J.; Lahiri, B.; Centrone A. Engineering near-field seira enhancements in plasmonic resonators. *ACS Photonics* **2016**, *3*, 87–95.

[49] Pięta, E.; Paluszkiewicz, C.; Oćwieja, M.; Kwiatek, W. M. Potential drug-nanosensor conjugates: Raman, infrared absorption, surface-enhanced Raman, and density functional theory investigations of indolic molecules. *Appl. Surf. Sci.* **2017**, *404*, 168–179.

[50] Purcell, S. M.; Barker, P. F. Tailoring the optical dipole force for molecules by field-induced alignment. *Phys. Rev. Lett.* **2009**, *103*, 153001.

[51] Yu, Y. Q.; Lin, K.; Zhou, X. G.; Wang, H.; Liu, S. L.; Ma, X. X. New C−H stretching vibrational spectral features in the Raman spectra of gaseous and liquid ethanol. *J. Phys. Chem. C* **2007**, *111*, 8971–8978.

[52] Leverette, C. L.; Jacobs, S. A.; Shanmukh, S.; Chaney, S. B.; Dluhy, R. A.; Zhao, Y.-P. Aligned silver nanorod arrays as substrates for surface-enhanced infrared absorption spectroscopy. *Appl. Spectrosc.* **2006**, *60*, 906–913.